

LU-TP 97-21  
NORDITA-97/54 P  
hep-ph/9709424  
September 1997  
Revised\* December 1997

# The Linked Dipole Chain Monte Carlo

Hamid Kharraziha  
Dept. of Theoretical Physics  
Sölvegatan 14a  
S-223 62 Lund, Sweden  
hamid@thep.lu.se

Leif Lönnblad  
NORDITA  
Blegdamsvej 17  
DK-2100 København Ø, Denmark  
leif@nordita.dk

## Abstract

We present an implementation of the Linked Dipole Chain model for deeply inelastic  $ep$  scattering into the framework of the ARIADNE event generator. Using this implementation we obtain results both for the inclusive structure function as well as for exclusive properties of the hadronic final state.

---

\*The original publication was based on results from an implementation containing an error. In this revised version this error has been corrected, some of the beyond leading-log assumptions have been revised and so have some of the results.

# 1 Introduction

With the HERA collider, a new kinematical regime has been opened up for studying deeply inelastic  $ep$  scattering (DIS) on partons carrying a very small momentum fraction  $x$  of the proton. Much theoretical and experimental effort has been made to increase our understanding of the dynamics of such small- $x$  partons, and much progress has been made, although many problems still need to be solved. On the theoretical side, a major issue is how to handle the resummation of large logarithms of  $x$  and  $Q^2$  in a consistent way, while a big obstacle for the experimental analysis has been the lack of theoretically well founded event generators which are able to describe the measurements made in this kinematical region.

The conventional way of describing the QCD evolution of the partons within a hadron, is to look at ladder diagrams where an incoming parton with large momentum and low virtuality undergo successive splittings, thus reducing its momentum and increasing its virtuality. The contributions from splittings where the parton retains only a small fraction  $z \ll 1$  of its momentum or where its virtuality is increased by a large factor  $\nu$ , are enhanced by large logarithms of  $1/z$  or  $\nu$  respectively, therefore such ladders need to be resummed to all orders.

The so-called DGLAP [1] evolution equations handles the resummation of logarithms of the virtuality by summing all ladder diagrams where the virtualities, or the transverse momenta  $k_\perp$ , are strongly ordered along the chain, while the BFKL [2] equations perform a  $\ln(1/z)$  resummation, summing ladders with strongly ordered momentum fractions, but unordered in  $k_\perp$ . Looking only at the inclusive structure function  $F_2$ , both of these approaches are able to explain the steep rise with  $1/x$  measured at HERA [3]. This is true also for the very small- $x$  region where the DGLAP equations are thought to be unreliable. However, the prediction from these approximations rely heavily on the assumption of the input parton distributions from which the evolution is started, and the absence of a small- $x$  enhancement in the evolution can be compensated with a steeply rising input distribution.

From the  $F_2$  measurement alone it is therefore difficult to estimate the relative importance of the different resummation approaches, and several suggestions have been made to instead look at different details of the hadronic final state to get a better understanding of the dynamics of QCD evolution [4]. Neither the BFKL or DGLAP equations are, however, suitable for describing non-inclusive event properties since that may destroy cancellations between real and virtual diagrams which are essential for the different approaches. In contrast, the so-called CCFM [5] evolution equations are designed to explicitly describe exclusive final-state properties by very carefully handling interferences between initial- and final-state splittings in the ladder, based on an angular ordered description. It can be shown to reproduce both the BFKL and DGLAP equations in their respective regions of validity.

To properly analyze measured properties of the hadronic final states found at HERA, it is important to have event generators which reproduce these properties to a satisfactory level. Unfortunately this has not been the case. The conventional generators, such as HERWIG [6] and LEPTO [7], are based on leading-log initial state parton showers derived from the DGLAP equations, and predict much too small partonic activity in the direction of the incoming proton (hereafter also referred to as the forward direction) for small- $x$  events [8,9]. This is expected, as the cascades are strongly ordered in transverse momenta, and are therefore limited by the smallness of  $Q^2$  in these events. In contrast, the dipole cascade implemented in the ARIADNE [10] program, where the generated partons are unordered in transverse momenta, is able to describe the final-state properties in the proton direction quite well. From this one may suspect that the resummation in the BFKL equations indeed are important, but since there is no clear relationship between the semi-classical soft radiation model [11] in Ariadne and the BFKL equation besides the  $k_\perp$  non-ordering, no firm statement can be made.

It is therefore important to construct an event generator implementing eg. the CCFM evolution, which can make reliable prediction about exclusive properties of the hadronic final state. Attempts has been made in this direction [12], but several difficulties have been encountered. A major obstacle with the CCFM equation is the presence of the so-called non-eikonal form factor which makes any implementation extremely inefficient.

Recently a reformulation of the CCFM equation has been proposed [13]. In this, the Linked Dipole Chain (LDC) model, the division between initial- and final-state radiation diagrams is redefined using the colour dipole cascade model (CDM). After this redefinition, the non-eikonal form factor drops out, which allows for a more simple implementation in an event generator.

A first attempt to construct such an event generator is presented in this paper. Although the LDC model is well suited for implementation in a Monte Carlo program there are a number of problems to be resolved. One problem is that both the CCFM and LDC models only deal with purely gluonic ladders while, to make a complete event generator, all types of ladders should be included. It is also important to handle energy-momentum conservation in a sensible way. Another important issue is the dependence on the input parton densities and the Sudakov form factors needed to regularize the poles in the splitting functions and to conserve the total momentum in the evolved parton density functions.

In section 2 we first recall the main ideas of the LDC model, then in section 3 we present the different issues involved in implementing the model in a Monte Carlo program. To obtain predictions for the hadronic final state we must first, as described in section 4, obtain input parton densities which together with the LDC evolution will give a satisfactory description of the inclusive cross section. Some results for the

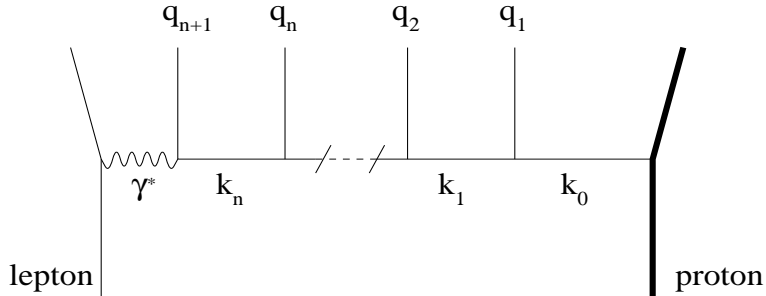


Figure 1: *Lepton proton scattering with  $n$  perturbative ISB emissions. The emitted ISB partons are denoted  $\{q_i\}$  and the propagators are denoted  $\{k_i\}$ .*

hadronic final state are then presented in section 5. Finally, our conclusions can be found in section 6.

## 2 The Linked Dipole Chain model

It is well known that the cross section for DIS events is not describable only by the lowest order perturbative terms. Still, it is not necessary to consider all possible emissions. A large set of them can be summed over and do, in principle, not affect the cross section. In the LDC model [13], the emissions that are considered to contribute to the cross section are regarded as Initial State Bremsstrahlung (ISB). The description of these emissions is based on the CCFM [5] model which is a leading-log approximation of the structure function evolution in DIS. The CCFM model has been modified by redefining which emissions should be counted as ISB, resulting in a much simplified description.

To describe final state properties of DIS events, one must also consider Final State Bremsstrahlung (FSB). In the LDC model this is done within the framework of the Colour Dipole cascade Model (CDM) [14] which has previously proved to give a good description of parton cascades in hadronic  $e^+e^-$  events and DIS. The general picture is that the initial parton ladder builds a chain of linked colour dipoles and that the FSB is radiated from these dipoles.

Let  $\{q_i\}$  denote the momenta of emitted partons,  $\{k_i\}$  denote the momenta of the propagators (see fig. 1) and  $z_{+i}$  be the positive light-cone momentum fraction<sup>1</sup> of  $k_i$  in each emission:  $k_{+i} = z_{+i}k_{+(i-1)}$ . According to the CCFM model, the emissions that contribute to the cross section (ISB) are ordered in rapidity and energy. Furthermore,

<sup>1</sup>Note that throughout this paper we work in the  $\gamma^*p$  centre of mass system with the proton along the positive  $z$ -axis, except in section 5 when comparing with experimental data, where the  $\gamma^*$  is along the positive  $z$ -axis.

there is a restriction on the transverse momenta of the continuing propagator in each emission:

$$k_{\perp i}^2 > z_{+i} q_{\perp i}^2. \quad (1)$$

The weight distribution,  $dw$ , of the initial chains factorizes, with the factors  $dw_i$  given by the following expression ( $\bar{\alpha} = 3\alpha_s/\pi$ ):

$$\begin{aligned} dw &= dw_1 dw_2 \cdots dw_n, \\ dw_i &= \bar{\alpha} \frac{dz_{+i}}{z_{+i}} \frac{d^2 q_{\perp i}}{\pi q_{\perp i}^2} \Delta_{ne}(z_{+i}, k_{\perp i}, q_{\perp i}). \end{aligned} \quad (2)$$

$\Delta_{ne}$  is the so called non-eikonal form factor, given by the expression:

$$\Delta_{ne}(z, k_{\perp}, q_{\perp}) = \exp \left[ -\bar{\alpha} \log \left( \frac{1}{z} \right) \log \left( \frac{k_{\perp}^2}{z q_{\perp}^2} \right) \right]. \quad (3)$$

In the LDC model, the definition of the ISB is more restricted. Consequently, more emissions are summed over and the expression for the weight distribution,  $dw_i$ , is changed. The new restriction is that in each emission, the transverse momentum ( $q_{\perp i}$ ) of the emitted parton must be larger than the lower one of the transverse momenta of the surrounding propagators

$$q_{\perp i} > \min(k_{\perp i}, k_{\perp(i-1)}). \quad (4)$$

In fig. 2 we show an example of an emission which belongs to the ISB according to the CCFM model but violates the restriction in eq. (4) and is regarded as FSB in the LDC model.

Summing over these emissions, the weight distribution of each allowed emission now becomes

$$dw_i = \bar{\alpha} \frac{dz_{+i}}{z_{+i}} \frac{d^2 q_{\perp i}}{\pi q_{\perp i}^2}. \quad (5)$$

This simplification of the expression for  $dw_i$  is due to the fact that one can interpret the non-eikonal form factor,  $\Delta_{ne}$ , as a Sudakov form factor, that is, it is equal to the probability of not violating the restriction in eq. (4).

By changing variables to the propagator momenta and integrating  $dw_i$  over the azimuthal angle (in the transverse plane) it can be written approximately as:

$$dw_i = \bar{\alpha} \frac{dk_{\perp i}^2}{k_{\perp i}^2} \frac{dz_{+i}}{z_{+i}} \min \left( 1, \frac{k_{\perp i}^2}{k_{\perp(i-1)}^2} \right). \quad (6)$$

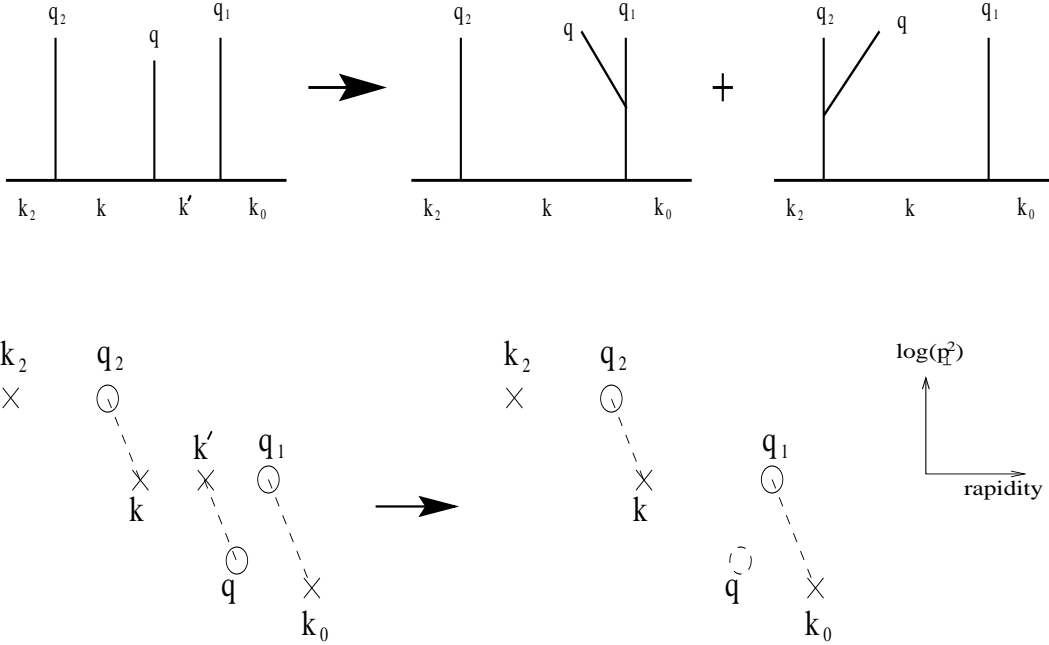


Figure 2:  $CCFM \rightarrow LDC$ : The emission  $q$  is regarded as ISB in the CCFM model but in LDC model it is regarded as FSB. This is illustrated (above) with fan diagrams and (below) in a  $\log p_{\perp}^2$ –rapidity diagram. Rapidity here is defined as  $\log(p_+/p_{\perp})$  and the dashed lines indicate equal  $p_+$ .

It is instructive to look at three different possibilities for two subsequent emissions, specified by different orderings of the transverse momenta of the propagators, numbered  $k_1$ ,  $k_2$  and  $k_3$  (with the same order as in fig. 1):

- $k_{\perp 1} < k_{\perp 2} < k_{\perp 3}$ : This is included in DGLAP and gives the same weight as there:  $dw_2 dw_3 \propto \frac{1}{k_{\perp 2}^2} \frac{1}{k_{\perp 3}^2}$ .
- $k_{\perp 1} < k_{\perp 2} > k_{\perp 3}$ : This gives the weight  $dw_2 dw_3 \propto \frac{1}{k_{\perp 2}^4}$  and resembles a hard sub-collision with a momentum transfer  $\hat{t} \simeq k_{\perp 2}^2$ .
- $k_{\perp 1} > k_{\perp 2} < k_{\perp 3}$ : Here  $dw_2 dw_3 \propto \frac{1}{k_{\perp 1}^2} \frac{1}{k_{\perp 3}^2}$ , it has no factor  $\frac{1}{k_{\perp 2}^2}$  and is thus infrared safe!

The LDC model, without corrections to the leading log approximation, has previously been studied and some qualitative results for the structure functions and final state properties in DIS have been presented in refs. [13, 15–17]. It is found that the LDC model, just as the CCFM model, interpolates smoothly between DGLAP and BFKL. The emissions along the rapidity axis can be separated in two phases: For rapidities closest to the proton (forward) direction, the ISB chain performs a

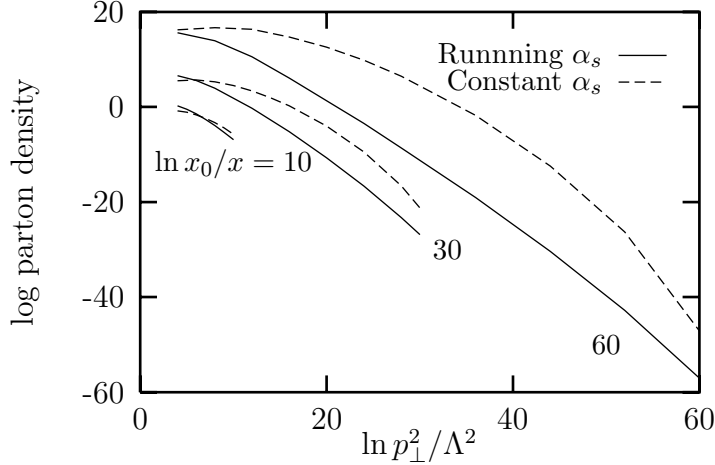


Figure 3: *The decrease of log of the parton density with  $\ln p_\perp^2$  at a certain rapidity, for different  $x$ -values, for running (solid line) and constant (dashed line) coupling.*

BFKL like motion with a constant mean  $E_\perp$ -flow. At a certain distance from the photon end, the transverse momentum of the emissions begins to rise to the photon virtuality, as expected by DGLAP. For the structure functions, a DGLAP behaviour ( $\exp(\text{const}\sqrt{-\log x})$ ) is shown for moderate values of  $x$ , but for small  $x$ -values it has the BFKL  $x^{-\lambda}$  behaviour.

A prediction from the BFKL model is that  $\log p_\perp$  of the emitted partons along the chain would be described by a Gaussian distribution with a growing width  $\propto \log 1/x$ . From the result of the LDC model, one can clearly see that this BFKL behaviour is indeed present for a constant coupling but not for a running coupling. This is illustrated in fig. 3 where the parton density at a certain rapidity is plotted as a function of  $\log p_\perp$  for different values of  $x$ -Bjorken, for constant and running coupling. The Gaussian behaviour is observed for constant coupling, while for a running coupling it appears to decay exponentially. It seems though that the exponential decay is significant only for events with very small  $x$ -values and will probably not be visible in currently available data.

The dipole model [14] was originally developed for final-state parton cascades from a quark-anti quark system. The phase space for gluon emission from a  $q - \bar{q}$  pair is approximately given by the triangular area in fig. 4a. The gluons are assumed to be radiated from a  $q - \bar{q}$  colour dipole and after each emission, the dipole is split into smaller dipoles (fig. 4b), which continue to radiate independently under a  $p_\perp$ -ordering condition (shaded area). Also  $g \rightarrow q + \bar{q}$  splittings have been included in this model. The size of the dipole triangle is determined by the total  $q - \bar{q}$  invariant mass  $W$ .

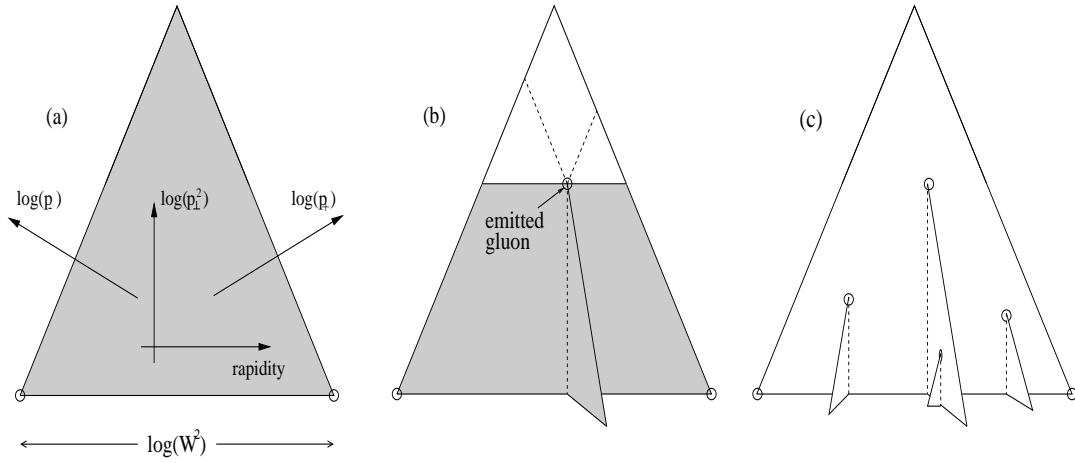


Figure 4: (a) The phase space of parton emission from a  $q - \bar{q}$  pair. (b) After the first emission, the phase space is split into two triangles which radiate gluons independently, but under a  $p_\perp$ -ordering condition. (c) An event with four emissions.

The momenta  $\{q_i\}$  of the emitted ISB partons in DIS are plotted in fig. 5a. Due to the ordering in positive and negative light cone momenta, one can insert the ISB into a dipole triangle with a size determined by the photon negative light cone momentum (left edge) and the positive light cone momentum of the incoming (non-perturbative) gluon (right edge). After doing this, the FSB partons can be emitted in a similar way as for the  $q - \bar{q}$  parton shower (fig. 5b). The phase space of the FSB is the shaded area in fig. 5a.

### 3 The Monte Carlo implementation

The LDC model has been implemented in a Monte Carlo program and some results within the leading log approximation have already been presented. Here we present a more complete implementation taking into account some non-leading corrections and generating complete events all the way down to the final state hadron level. What follows is a step-by-step description of the procedure.

The basic formula for the evolution of the parton densities is

$$x f_i(x, Q^2) = \sum_j \int_x^1 \frac{dx_0}{x_0} [ G_{ij}(x, Q^2, x_0, k_{\perp 0}^2) + S_j(Q^2, k_{\perp 0}^2) \delta_{ij} (\ln x - \ln x_0) ] x_0 f_{0j}(x_0, k_{\perp 0}^2), \quad (7)$$

Where  $G_{ij}(x, Q^2, x_0, k_{\perp 0}^2)$  is the sum of the weights of all chains starting with a parton  $j$  at some low scale  $k_{\perp 0}^2$  carrying a momentum fraction  $x_0$ , and ending up with a

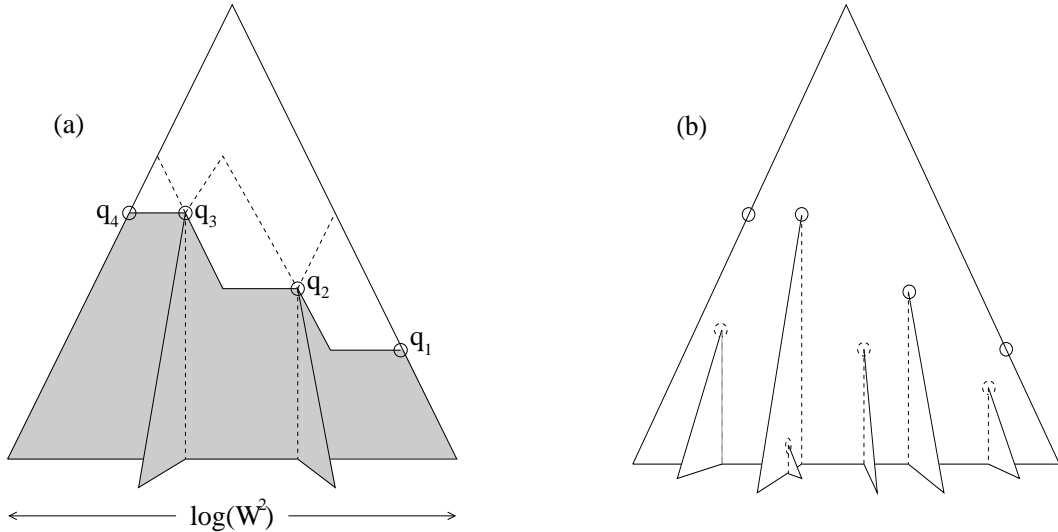


Figure 5: (a) ISB emissions plotted in a dipole triangle. (b) The solid circles are ISB emissions and the dashed circles are FSB emissions.

parton  $i$  carrying a momentum fraction  $x$  being hit by a photon with virtuality  $Q^2$ . The delta function corresponds to the case of no emissions.  $G$  is positive definite, and to conserve the total momentum,  $\sum_j \int_0^1 x f_j(Q^2, x) dx = 1$ , the delta function is multiplied by a Sudakov form factor,  $S_j(Q^2, k_{\perp 0}^2)$ , representing the probability that the parton  $j$  with momentum fraction  $x_0$  at  $k_{\perp 0}^2$  has not split, and thus reduced its momentum, when probed at a higher scale  $Q^2$ . This form factor will be discussed in detail below.

The analytic approximate upper limiting function for  $G$  [15], given by

$$G_{ij}(x, Q^2, x_0, k_{\perp 0}^2) \lesssim G(Q^2/k_{\perp 0}^2, x/x_0) = \sqrt{\frac{a}{b}} I_1(2\sqrt{ab}) \quad (8)$$

$$a = \sqrt{\bar{\alpha}}(\ln Q^2/k_{\perp 0}^2 + \ln x_0/x), \quad b = \sqrt{\bar{\alpha}} \ln x_0/x$$

provides us with the starting point, and for each generated chain  $c$  a number of multiplicative weights are calculated  $\omega_c = \prod_l \omega_c^{(l)}$  so that the correct form of  $G_{ij}$  is obtained as

$$G_{ij}(x, Q^2, x_0, k_{\perp 0}^2) = \bar{\omega}_{ij}(x, Q^2, x_0, k_{\perp 0}^2) G(Q^2/k_{\perp 0}^2, x_0/x), \quad (9)$$

with the average weight

$$\bar{\omega} = \frac{1}{N} \sum_{c=1}^N \omega_c \quad (10)$$

This is how it is done:

1. First the  $x$ ,  $Q^2$  and the flavour  $i$  of the struck quark is chosen using evolved parton densities and the standard Born-level electro-weak matrix elements. This is currently done within the LEPTO program [7].
2. Then the  $x_0$  and flavour of the incoming parton is chosen according to eqs. (7) and (8) with  $k_{\perp 0}$  as a given parameter.
3. The number of emissions is chosen from

$$\sqrt{\frac{a}{b}} I_1(2\sqrt{ab}) = \sum_{n=1}^{\infty} \frac{a^n b^{n-1}}{n!(n-1)!} \quad (11)$$

4. The positive and negative light-cone momentum fractions,  $z_{j+}$  and  $z_{j-}$  which enters in each emission  $j$  is generated according to the ordered integral

$$\frac{a^n b^{n-1}}{n!(n-1)!} = \int \bar{\alpha}^n \Pi_j \frac{dz_{j+}}{z_{j+}} \frac{dz_{j-}}{z_{j-}} \delta(\ln x_0 + \sum_j \ln z_{j+} - \ln x) \quad (12)$$

5. At this point we need to choose the flavours of each link. To do this we introduce the standard Altarelli-Parisi splitting functions and preliminary we use their approximations,  $\tilde{P}_{i \rightarrow j}(z)$ , in the  $z \rightarrow 0$  limit

$$\begin{aligned} P_{q \rightarrow q}(z) &= C_F \frac{1+z^2}{1-z} \approx C_F, \\ P_{g \rightarrow g}(z) &= 2N_C \frac{(1-z)(1-z)^2}{z(1-z)} \approx 2N_C \frac{1}{z}, \\ P_{g \rightarrow q}(z) &= T_R(z^2 + (1-z)^2) \approx T_R, \\ P_{q \rightarrow g}(z) &= C_F \frac{1+(1-z)^2}{z} \approx C_F \frac{2}{z}, \end{aligned} \quad (13)$$

We get the first weight factor as the approximated splitting functions summed over all possible flavour combinations,

$$\omega^{(0)} = \sum \Pi \frac{\tilde{P}_{i \rightarrow j}(z_+)}{\tilde{P}_{g \rightarrow g}(z_+)} \quad (14)$$

6. We can then use eq. (14) to generate a specific flavour combination according to their individual weights.
7. Next, we generate the azimuthal angles of each emission and construct the exact kinematics. The delta function in eq. (12), which handles the conservation of positive light-cone momenta, does not take into account the transverse degrees of freedom. In particular it would give zero positive light-cone momentum

for the struck quark,  $q_{n+1}$ , in the final-state. We therefore modify this delta function to exactly conserve the total energy and momentum, effectively setting  $z_{n+}$  by hand to the value needed. However, for some values of the azimuth angles this is not possible and we get a weight factor corresponding to the allowed integration area  $\Delta\phi_j$ :

$$\omega^{(1)} = \Pi_j \frac{1}{2\pi} \int_{\Delta\phi_j} d\phi_j. \quad (15)$$

8. Then we implement the condition that the transverse momenta (which is generalized to the transverse mass  $m_\perp$  for massive partons) of an emitted parton must be larger than the smallest virtuality  $v_{j \min}$  of the connecting links  $j$  and  $j-1$ , and that all virtualities must be above  $k_{\perp 0}^2$ , giving us the second weight factor

$$\omega^{(2)} = \Pi_j \Theta(m_{\perp j}^2 - v_{j \min}) \Theta(v_{j \min} - k_{\perp 0}^2). \quad (16)$$

We note that the weights are finite even if one of  $v_j$  and  $v_{j-1}$  goes to zero, and one could imagine replacing the second theta function in eq. (16) with  $\Theta(v_{j \max} - k_{\perp 0}^2)$ . This would reduce the dependency on  $k_{\perp 0}$  and would allow for more unordered chains as discussed below.

9. Now we introduce the running of  $\alpha_s$ , giving a fourth weight

$$\omega^{(3)} = \Pi_j \frac{1}{\ln(m_{\perp j}^2/\Lambda^2)} \quad (17)$$

10. Having obtained the virtualities of the links, we can now correct the splitting functions in eq. (14). We get the following cases:

- $v_{j+1} > v_j > v_{j-1}$ : Going upwards from the proton side we use  $P_{f_{j-1} \rightarrow f_j}(z_{j+})$
- $v_{j+1} < v_j < v_{j-1}$ : Going upwards from the photon side we use  $P_{f_{j+1} \rightarrow f_j}(z_{j-})$
- $v_{j+1} < v_j > v_{j-1}$ : Corresponds to a Rutherford scattering and  $z_{j+} \approx z_{j-} \equiv z$ . Here we use  $2 \rightarrow 2$  matrix elements taking into account colour connections as explained in Appendix A.
- $v_{j+1} > v_j < v_{j-1}$ : Here we use the  $z \rightarrow 0$  limit,  $\tilde{P}_{i \rightarrow j}(z)$  of the splitting functions, where  $z = z_+$  if  $v_{j+1} > v_{j-1}$  or else  $z = z_-$ .

Note that the colour factor is independent of the ordering of the virtualities. Therefor we have to correct for only the kinematical part of the splitting function by using reduced splitting functions  $\tilde{P}$  where the colour factor is divided out. Here we also introduce the Sudakov form factor, to be discussed below and we can write the fourth weight factor

$$\omega^{(4)} = \Pi_j \frac{S_j(v_{j-1}, v_j, v_{j+1}) \tilde{P}_{f_{j-1} f_j f_{j+1}}^{v_{j-1} v_j v_{j+1}}(z_{j+}, z_{j-})}{\tilde{P}_{f_{j-1} \rightarrow f_j}(z_{j+})}, \quad (18)$$

where  $S_j(v_{j-1}, v_j, v_{j+1})$  is  $S_{f_{j-1}}(v_j, v_{j-1})$  or  $S_{f_{j+1}}(v_j, v_{j+1})$  depending on whether the virtuality is going up or down.

$P_{q \rightarrow q}$  and  $P_{g \rightarrow g}$  both have poles as  $z \rightarrow 1$ , corresponding to emission of low-energy gluons. Typically these should be counted as final-state emissions, but to be sure to avoid divergences we introduce a cutoff  $z_{\text{cut}} = 0.5$ . See also the discussion of double counting below.

Note also that we use mass less splitting functions, and the production of heavy quarks is only suppressed by the phase space. This should be improved in the future.

11. The final weight factor is introduced to correct the emission closest to the photon, in the cases where  $v_n > v_{n-1}$ , to reproduce the exact  $\mathcal{O}(\alpha\alpha_s)$  matrix element as given eg. in ref. [18]:

$$\omega^{(5)} = \frac{\mathcal{M}(Q^2, x, z_{n+}, z_{n-})}{P_{f_{n-1}f_n\gamma}^{v_{n-1}v_nQ^2}(z_{n+}, z_{n-})} \quad (19)$$

12. The generated chain is now kept with a probability  $\omega_c = \frac{1}{W} \Pi_l \omega_c^{(l)}$ , where  $W$  is a scale factor to avoid probabilities larger than one. There is in principle nothing preventing weight larger than one, but they turn out to be very rare. Nevertheless, it may happen, and it is important to check that  $W$  is large enough so that the results are not influenced by this. Chains with  $\omega > 1$  may optionally be saved and retrieved again when an event with the same flavour and similar  $x$  and  $Q^2$  is requested. A chain will then be used on the average  $\omega_c$  times, each time with different final-state cascade and hadronization. Below we have used  $W = 1$  giving less than 0.1% events with weight larger than one.
13. To prepare for the final-state dipole radiation the emitted partons must be connected together and form dipoles. In the case of quark links, this is straight forward, the incoming quark is simply connected to the first emitted gluon and so on until the struck quark. In the case of gluon links, there are two colour lines, and a radiated gluon can belong to either of these. This choice is done completely at random. The connection between the colour line of the incoming parton and the proton remnant is handled in the same way as in the default soft radiation model of ARIADNE [10].

One could imagine using other methods for determining the colour-flow. One suggestion is to use the colour-flow which minimize the total string length<sup>2</sup>. One could also consider colour-reconnections, following eg. the model already implemented in ARIADNE [20], possibly giving rise to large rapidity gaps among the final-state hadrons.

---

<sup>2</sup>As defined eg. by the  $\lambda$  measure of ref. [19]

14. The constructed dipoles can then radiate more final-state gluons in the phase-space limited by the virtuality and the positive and negative light-cone momenta of the links in the chain as in fig. 5a. Note that also in the no-emission case corresponding to the delta function in eq. (7), some radiation is allowed within the triangular area defined by  $q_+ < -Q_+$  and  $q_- < Q_-$ . In the Breit frame, this is just the area of allowed FSB in a  $e^+e^- \rightarrow q\bar{q}$  event with centre of mass energy  $Q$ .
15. Finally the final state dipole chains are hadronized according to the Lund string fragmentation model as implemented in JETSET [21].

This concludes the description of the actual implementation. But before we can start producing events we have to fix the parameters involved. These are  $\Lambda$ ,  $k_{\perp 0}$ ,  $W$ ,  $z_{\text{cut}}$  and the input parton densities  $x_0 f_{0j}(x_0, k_{\perp 0}^2)$ .  $W$  is not really a physical parameter, and should be set large enough so that the result no longer depend on it. It would be natural to take  $\Lambda$  and  $k_{\perp 0}$  to be the values which have been tuned for the final state dipole cascade to reproduce LEP data,  $\Lambda_{\text{LEP}}$  and  $k_{\perp 0\text{LEP}}$ . One could, of course, use an increased cutoff  $k_{\perp 0} > k_{\perp 0\text{LEP}}$  in the ISB. This would mean that more emissions would be moved from the initial to the final state, which would continue emitting down to  $k_{\perp 0\text{LEP}}$ . We therefore expect the final result to be fairly stable w.r.t. such variations as long as  $k_{\perp 0}$  is not too large.

There is an additional complication with a large  $k_{\perp 0}$  for the cases where the virtuality drops below  $k_{\perp 0}$  somewhere along the chain, causing a zero weight in eq. (16). For the total cross section, this does not matter, as such fluctuations are included in the input parton densities at a lower  $x_0$ , corresponding to the momentum fraction of the link closest to the photon which is below the cutoff. For the final state, however, it means that we are excluding some radiation close to the direction of the incoming hadron.

As discussed above, one could replace the second theta function in eq. (16) with  $\Theta(v_{j\max} - k_{\perp 0}^2)$  since the  $m_{\perp}^2$  then would still be in the perturbative region. In this way the result would be less sensitive to variations of  $k_{\perp 0}$ , as the perturbative system on the proton side of the sub-cutoff link would still be generated. This would not, of course, solve the problem altogether as one can imagine chains where two or more consecutive links are below the cutoff.

In step 10 we have replaced the  $N_c/z$  pole, which is used in the emissions of the original leading log LDC model, with the standard Altarelli-Parisi splitting functions. This should be a sensible way of including some sub-leading effects, as long as the splitting functions are regularized in a correct way. In each emission, two particles are produced and one vanishes. For the parton distributions, this means we must subtract and add partons correspondingly.

A simple way of treating this double counting problem is to add only one of the

produced partons assuming that the mother parton is not affected by the emission. The choice of which of the two partons to add is not trivial. One way is to introduce a cut-off  $z_{cut} = 0.5$  allowing only  $z < z_{cut}$ . This is a good choice in the  $g \rightarrow g$  splitting since the gluon with  $z > 0.5$  is more similar to the mother gluon. For the other emissions, which involve both quarks and gluons, it is more important to make the choice which leads to a better approximation of the quark distributions. This can be done by allowing all  $q \rightarrow g$  splittings, forbidding all  $q \rightarrow q$  splittings and allowing  $g \rightarrow q$  splittings only if the quark (or anti-quark) interacts directly with the photon.

In a more sophisticated treatment, the subtraction of a parton is done with Sudakov form factors corresponding to the probability for the partons not to vanish before the splitting can occur. In this way, we can take into account that e.g. the possibility for a gluon to split into a quark anti-quark pair with low virtuality reduces its contribution to emissions with higher virtualities. The suppression factor becomes an exponential of an integral over the splitting

$$S_g = \exp \left[ - \int_0^1 P_{g \rightarrow q}(z) dz \int \frac{\alpha_s(q_\perp^2)}{2\pi} \frac{dq_\perp^2}{q_\perp^2} \right]. \quad (20)$$

The region of integration corresponds to the region of allowed emissions. Here we only use an approximate form. A more thorough investigation will be presented in a future paper.

The lower limit on  $q_\perp^2$  is given by the lowest virtuality of an emission step multiplied by a fudge factor,  $e^\delta$ , to account for the suppression of the emission probability for small  $q_\perp$ -values (eq. (4)). The value of  $\delta = 0.4$  that is used has proven to be an effective cut-off in the leading log treatment of the LDC model [15, 17]. The upper limit is set to the highest virtuality of an emission step. One could imagine having a higher, or a  $z$  dependent limit, but for simplicity we only use the virtuality in this publication.

The Sudakov factor due to the  $g \rightarrow g$  splitting depends on the choice of  $z_{cut}$ . For  $z_{cut} = 0.5$ , there is no double counting to correct for and for larger  $z_{cut}$  the integration of the splitting function is in the region  $0.5 < z < z_{cut}$ . If  $q \rightarrow q$  splittings are allowed, quarks are suppressed with a Sudakov factor where the integration region is given by  $0 < z < z_{cut}$ .

The situation is quite different when we are interested in the final state properties. Here, the Sudakov form factors are not as important since they for most events roughly give an overall factor  $\prod_{j=1}^n S(v_{j-1}, v_j, v_{j+1}) \sim S(k_{\perp 0}^2, Q^2)$  which does not have an influence on the relative contributions of different final states. On the other hand, disallowing some of the initial state emissions to reduce double counting has a large effect on the final state properties since it reduces high  $p_\perp$  emissions. This is a problem except for gluon emissions with  $z > 0.5$  in regions with ordered virtuality,

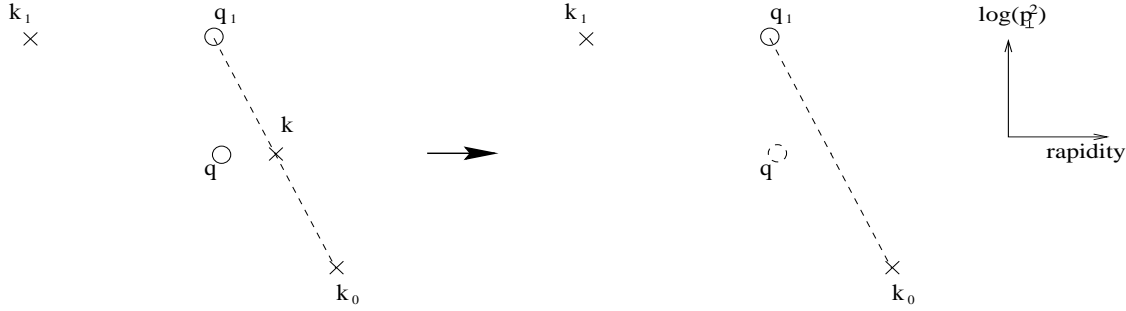


Figure 6: *In the case where the virtuality is increasing, a splitting with  $z$  larger than 0.5 corresponds to an emission of a gluon  $q$  which is inside the phase space where subsequent FSB emissions is allowed. Such splittings should therefore be removed from the ISB chains to avoid double counting.*

since these gluons can be treated as final state emissions as shown in fig. 6. Consequently, we would expect it to be a good approximation for the final state generation to skip the Sudakov form factors and to allow some of the splittings which lead to double counting.

It is clear that the result is very dependent on the non-perturbative input parton densities, which are basically unknown. If eg. the gluon density is very divergent at small  $x$ , the  $x_0$  chosen from eq. (7) will tend to be small, limiting the total phase space available for radiation  $\Delta y \propto \ln x_0/x$ . The input parton densities can, however, be constrained somewhat from the total cross section, and we can parametrize them and make a fit of the parameters to eg.  $F_2$  data at different  $x$  and  $Q^2$ .

## 4 Fitting the input parton densities

From eq. (7) we can write the leading order expression for  $F_2$  as

$$F_2 = \sum_{i \neq 0} e_i^2 \sum_j \int_x^1 \frac{dx_0}{x_0} [ G_{ij}(x, Q^2, x_0, k_{\perp 0}^2) + S_j(Q^2, k_{\perp 0}^2) \delta_{ij} (\ln x - \ln x_0) ] x_0 f_{0j}(x_0, k_{\perp 0}^2). \quad (21)$$

For given values of  $x$ ,  $Q^2$ ,  $x_0$ ,  $k_{\perp 0}^2$ ,  $i$  and  $j$ , we can calculate  $G_{ij}(x, Q^2, x_0, k_{\perp 0}^2)$  from steps 3 through 11 in the previous section using eq. (9). For any given parametrization of the input densities it is then possible to calculate  $F_2$  and compare with experimental data.

In principle one could also fit to other data, such as prompt photon and jet production

in hadron-hadron collisions. This is not possible in our current implementation which only gives the evolved densities for quarks and anti-quarks. This means that the input gluon distribution is only constrained indirectly from the  $Q^2$  dependence of  $F_2$ , and in this paper we only make a very crude fit using only four different parameters for  $x_0 f_{0j}(x_0, k_{\perp 0}^2)$ .

The input densities are parametrized as

$$x f_{0j}(x) = A_j x^{\alpha_j} (1 - x)^{\beta_j}. \quad (22)$$

For the valence distributions  $u_v(x)$  and  $d_v(x)$  we use the same form, with  $\beta_v = 3$  leaving  $\alpha_v$  free and using the normalization

$$\int_0^1 u_v(x) dx = 2, \quad \int_0^1 d_v(x) dx = 1 \quad (23)$$

to fix  $A_{uv}$  and  $A_{dv}$ . For the gluon distribution,  $\beta_g = 4$  while  $\alpha_g$  and  $A_g$  are left free. All the sea-quarks distributions have the same form with  $\beta_S = 4$ , leaving  $\alpha_S$  free and setting  $2A_s = 2A_{\bar{s}} = A_u = A_{\bar{u}} = A_d = A_{\bar{d}}$  so that the total momentum

$$\int_0^1 dx \sum_j x f_{0j}(x) = 1 \quad (24)$$

is conserved.

We only use data from proton  $F_2$  measurements from H1 [22], ZEUS [23], NMC [24] and E665 [25] without allowing for any normalization uncertainty factors. We use only data for  $Q^2 > 1.5$  GeV and  $x < 0.5$  to ensure a reasonable length of the evolution. We then make six sets of fits using different options in the generation of the  $G$  function:

- A LDC default:  $k_{\perp 0} = 0.6$  GeV,  $\Lambda = 0.22$  GeV.
- B DGLAP: As for A but only allow chains with monotonically increasing virtualities of the links from the proton side.
- C DGLAP': As for B, but chains where the virtuality of the link closest to the virtual photon is larger than  $Q^2$  are permitted. We use this as a kind of higher-order corrected DGLAP evolution although, of course, not equivalent to NLO evolution.
- D As for A but  $k_{\perp 0} = 1$  GeV, to check the sensitivity to this cutoff.
- E As for A but without the Sudakov form factor. Instead  $P_{q \rightarrow q}(z)$  is set to zero and  $P_{g \rightarrow q}(z)$  is nonzero only in the splitting closest to the photon.

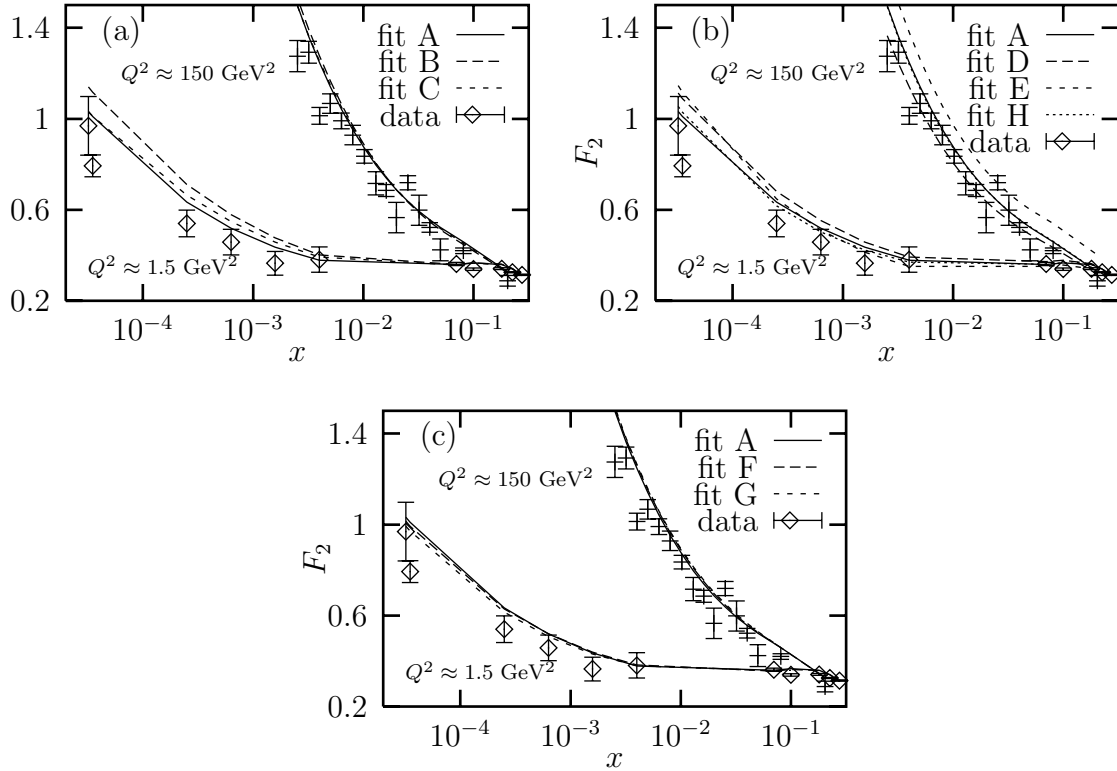


Figure 7: The fitted  $F_2$  as a function of  $x$  for different strategies and for two different values of  $Q^2$ , compared with data from [22–25].

- F As for A but  $\beta_g = \beta_S = 5$  to check the sensitivity to the fit parameters.
- G As for A but only fitting to  $F_2$  data with  $x < 0.1$ , to reduce the sensitivity to the step size  $\delta \ln x_0/x = 0.2$  used when integrating eq. (21), and to the high- $x$  form of the input parametrization.
- H As for A but allow the virtuality of some links to be below  $k_{\perp 0}$  as long as the largest virtuality of two consecutive links always is above  $k_{\perp 0}$ .

The results of the fits are presented in figs. 7 and 8. For the default case, the fit is quite acceptable. We note in particular that the fitted input gluon density is slowly decreasing with  $1/x$ , although we must keep in mind that the gluon distribution is only indirectly constrained.

For the DGLAP case the fit is much worse. The number of allowed ISB emissions is here strongly restricted, especially for small  $Q^2$  and  $x$ . This results in much slower evolution which forces the input densities to rise with  $1/x$ . In fit C, where the link closest to the virtual photon is allowed to be above  $Q^2$ , the fit is on the other hand again quite acceptable. The input gluon distribution is no longer rising with  $1/x$ ,

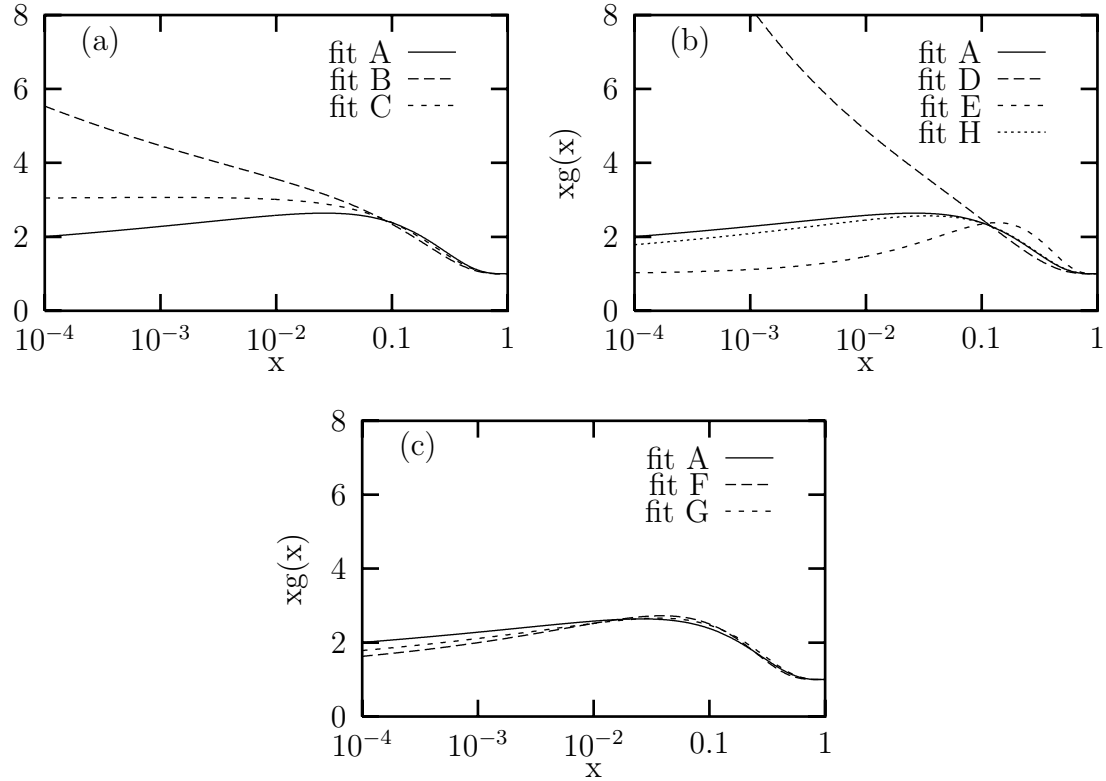


Figure 8: *The fitted input gluon density as a function of  $x$  for different strategies.*

on the other hand it is as strongly decreasing as in fit A. It is known that  $F_2$  can be fitted using conventional DGLAP evolution with a valence-like flat input distribution at small input scales, close to the one used here, as in the GRV parametrizations [26]. Such fits can, however, not be directly compared to this one, as we here have less parameters. But we can conclude that the ISB chains with unordered  $k_\perp$  do play a rôle in our case, although most of the effect can be obtained allowing only for one ‘stepping down’, closest to the photon in the chain.

Increasing the input scale to 1 GeV in fit D makes a big difference particularly at small  $x$  as seen in figs. 7b and 8b. Also here the number of allowed ISB emissions is strongly restricted and again the input gluon is forced to increase strongly with  $1/x$ . This should come as no surprise. We expect, however, that when we below study the hadronic final states, the result should be less sensitive to the input scale used.

The importance of the Sudakov form factor is apparent in figs. 7b and 8b, comparing fits A and E, especially for the input gluon distribution. Also in figs. 7b and 8b we show the fit H, where some propagators below the cutoff is allowed. The reproduction of  $F_2$  does not change much, but we see that the input gluon decreases slightly faster with  $1/x$  than for the default fit A.

The fits F and G in figs. 7c and 8c show how sensitive the fit is to the input distribution at large  $x$ . Changing  $\beta_g$  and  $\beta_S$  from 4 to 5 does not influence the fit very much and neither does the omission of the data points at high  $x$ , although in both cases the input gluon is shifted somewhat to higher  $x$ .

## 5 Results for the hadronic final states at HERA

The results for the hadronic final states will depend on the input densities used. If eg. the input densities are increasing with  $1/x_0$ , chains starting with low  $x_0$  will be favoured and the length of the chains will be shorter resulting in fewer emissions and less activity in general due to the reduction of the available phase space, in particular close to the direction of the incoming hadron. Also a smaller input gluon density will result in fewer chains initiated with a gluon, which has higher charge than an incoming quark, and again the probability of emissions will become smaller. In addition, the non-perturbative hadronization is smaller if only one string is stretched between the perturbative system and the hadron remnant in the case of an incoming quark.

To study the hadronic final states we use the HZTOOL package [27] developed jointly by H1, ZEUS and theoreticians for comparison between event generators and published experimental data. We have selected six different distributions which have been shown to be sensitive to details in the models used in Monte Carlo event generators. The distributions presented in fig. 9, which are all measured in the hadronic centre of mass system, are as follows.

- (a) The  $E_\perp$ -flow as a function of the pseudo rapidity for two bins in  $x$  and  $Q^2$ , one with low  $x$  and low  $Q^2$ , and one with moderate  $x$  and  $Q^2$  in (b) [8]. The large amount of  $E_\perp$  in the forward direction was previously claimed to be a good signal of  $k_\perp$  non-ordering in the ISB, but it has been shown that this effect can also be obtained by the introduction of additional non-perturbative effects.
- (c) The so-called seagull plot with the average  $k_\perp^2$  as a function of Feynman- $x$  [28], which at eg. EMC [29] was shown to be difficult to reproduce with event generators.
- (d) The  $k_\perp$ -distribution of charged particles in a forward pseudo rapidity bin. This was recently proposed [9, 31] as a new signal for perturbative activity in the forward region indicating  $k_\perp$  non-ordering: a high- $k_\perp$  tail would be difficult to reproduce by non-perturbative models, where such tails would be exponentially suppressed.
- (e) In [9] was also shown that the pseudo rapidity distribution of charged particles with  $k_\perp > 1$  GeV also could be a good signal for  $k_\perp$  non-ordering.

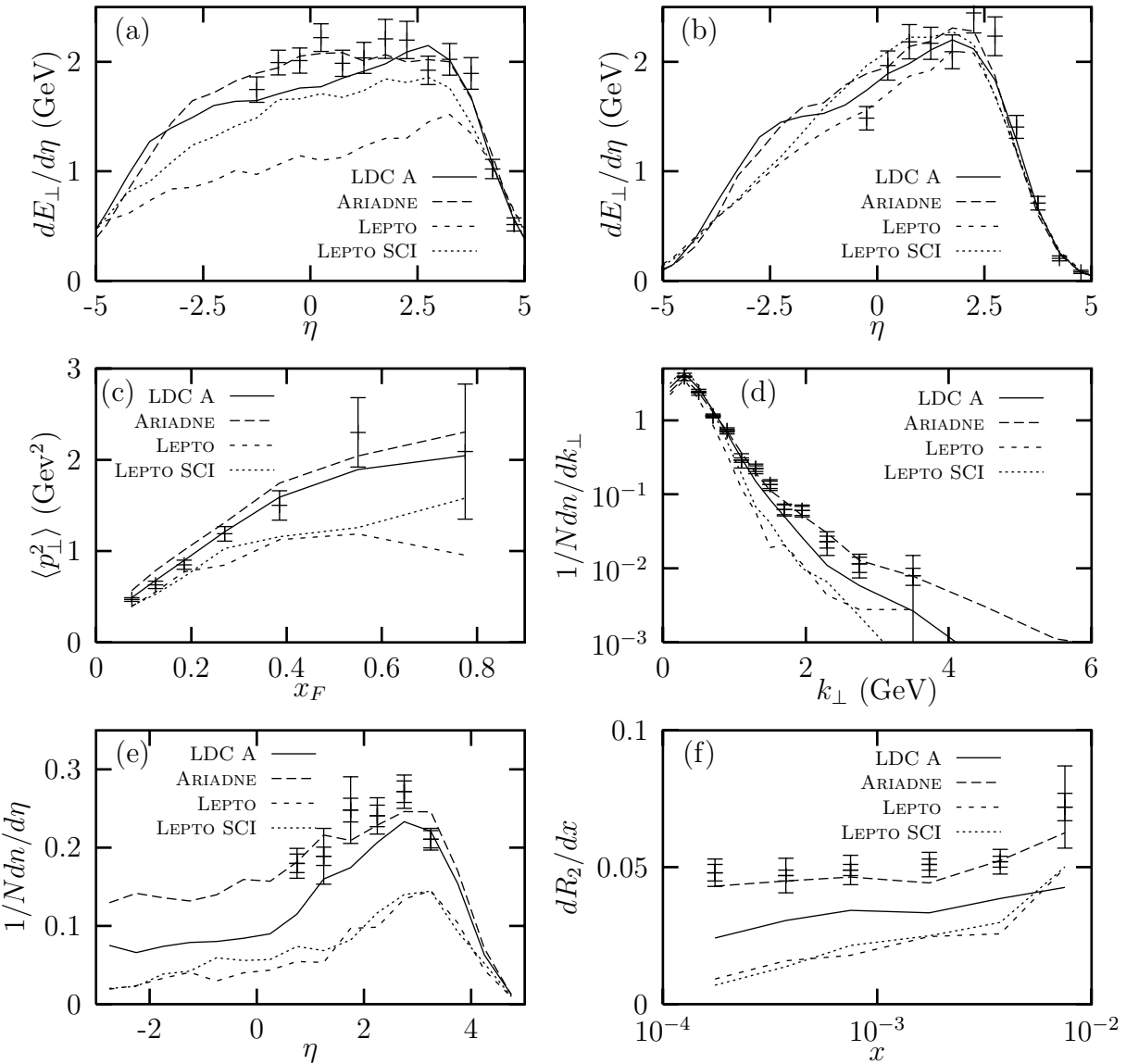


Figure 9: Comparison of the default LDC A model with HERA data as given in [27] and other event generators. The distributions are as follows: (a) The transverse energy flow as a function of pseudo rapidity for events with  $0.0001 < x < 0.0002$ ,  $5 < Q^2/\text{GeV}^2 < 10$  [8]. (b) As (a) but for events with  $0.003 < x < 0.01$ ,  $20 < Q^2/\text{GeV}^2 < 50$ . (c) The average squared transverse momentum of charged particles as a function of  $x_F$  [28]. (d) The transverse momentum distribution of charged particles in the pseudo rapidity bin  $0.5 < \eta < 1.5$  for events with  $0.0002 < x < 0.0005$ ,  $6 < Q^2/\text{GeV}^2 < 10$  [9]. (e) The pseudo rapidity distribution of charged particles with a transverse momentum larger than 1 GeV for the same kinematical bin as in (d). (f) The two-jet ratio  $R_2(x)$  as a function of  $x$  [30]. All measurements were made in the hadronic centre of mass system and only events without a large rapidity gap were included. The full line is LDC A, long-dashed is ARIADNE 4.08 with default parameter settings, dotted is LEPTO 6.4 with default parameter settings and short-dashed is the same but with SCI and the special sea-quark remnant treatment [32] switched off.

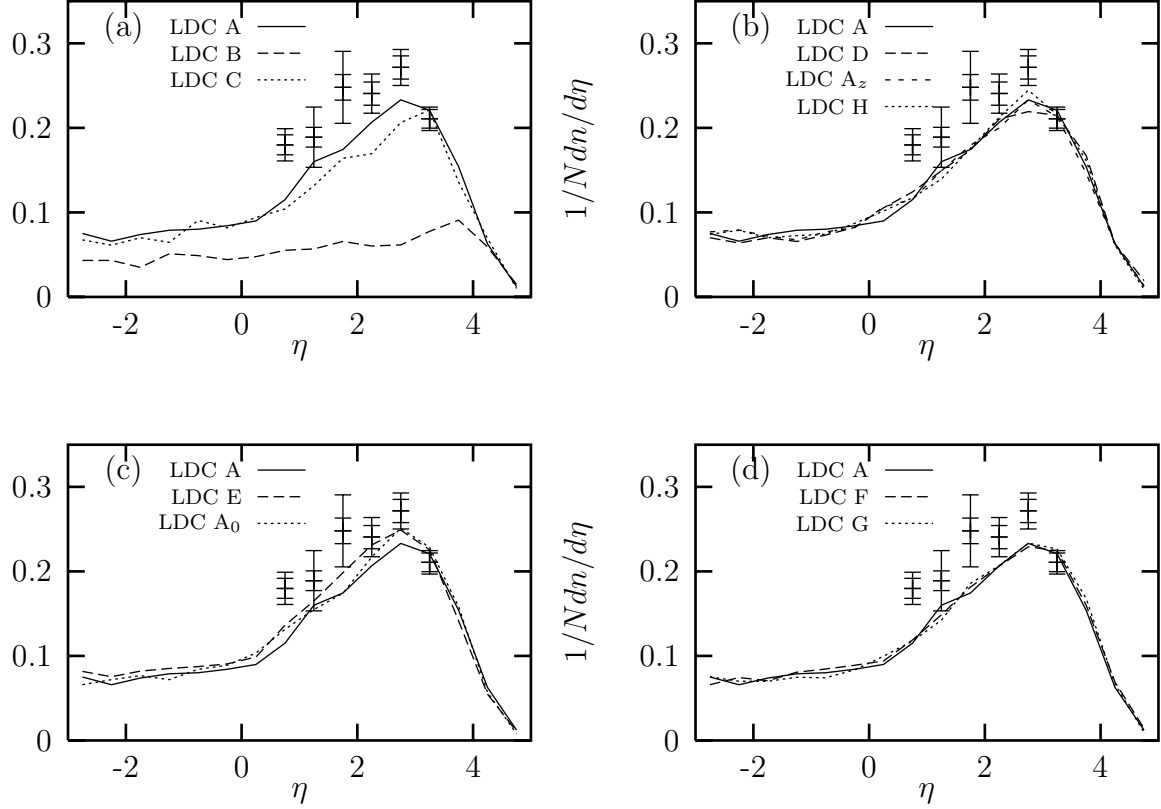


Figure 10: *Comparison between different LDC strategies and data corresponding to fig. 9e. In all cases the full line is the default LDC A strategy. In (a) the dashed line is LDC B using only DGLAP-like chains and dotted is LDC C, i.e. the same but allowing the virtuality of the link closest to the photon to be above  $Q^2$ . In (b) the long-dashed line is LDC D with  $k_{\perp 0} = 1$  GeV, the short-dashed is LDC  $A_z$  with increased cutoff,  $z_{cut}$ , in the splitting functions and dotted is LDC H, allowing some propagators below the cutoff. In (c) the dashed line is LDC E without Sudakov form factors and disallowing all  $q \rightarrow q$  and most  $g \rightarrow q$  splittings in the parton density fit and the dotted, LDC  $A_0$ , is the same as LDC A but using Sudakov only in the parton density fit. Finally in (d) the dashed line is LDC F using a different form of the input densities at large  $x$  and the dotted is LDC G restricting the fit to  $F_2$  data with  $x < 0.1$ .*

- (f) Result for the two-jet ratio  $R_2$  was recently reported [30] and showed large differences between the currently used event generators.

In fig. 9 we see the results from LDC with default settings and using fit A, labeled LDC A, compared with data and with the results for ARIADNE using the default soft radiation model, with LEPTO with and without the additional non-perturbative (soft colour interactions (SCI), and perturbative-like treatment of remnants in the case of sea quarks) assumptions presented in [32]. For the ARIADNE and LEPTO models we confirm previous results where ARIADNE, which until now was the only model implementing  $k_\perp$  non-ordering, reproduces the data very well while the DGLAP-based LEPTO has difficulties, especially without the additional non-perturbative models. We find that the result for LDC is quite acceptable, although not reproducing data as well as ARIADNE.

To compare different LDC strategies, we show in fig. 10 only the number of charged particles with transverse momentum larger than 1 GeV as a function of pseudo rapidity for small  $x$  and  $Q^2$  (fig. 10). The effects on the other distributions in fig. 9 are very similar.

In fig. 10a we see the results for LDC when restricting to DGLAP-like chains. In this case, corresponding to the lines marked LDC B, the result is very poor as expected. Allowing the virtuality of the link closest to the photon to be above  $Q^2$  as for LDC C, makes things much better and only slightly worse than the default LDC A. Naïvely one may expect this to give the same result as LEPTO which uses the exact  $\mathcal{O}(\alpha_s)$  Matrix Element for the emission closest to the photon, also allowing the first link to have a virtuality larger than  $Q^2$ , and which adds on parton-showers à la DGLAP on such configurations. But in LDC, even though no ISB emissions are allowed between the highest virtuality link and the photon, there is still a resummation of diagrams which are then replaced by FSB emissions. LEPTO, however, uses the 'bare' matrix element and does not include any resummation.

For the line marked LDC D in fig. 10b, the cutoff in  $k_\perp$  for the ISB is set to 1 GeV. In the previous section we saw that the parton density functions in this case became dramatically different. For the final state, however, the reduction of ISB is compensated by final state dipole emissions, which are allowed in the whole rapidity range below  $k_\perp = 1$  GeV down to the cutoff fitted to LEP data,  $k_{\perp 0\text{LEP}} = 0.6$ . The effect of increasing  $z_{\text{cut}}$  is also shown in fig. 10b for the line LDC  $A_z$ . The dependence on this cutoff is small, which is expected as most of the emissions with  $z > 0.5$  are counted as FSB as explained in fig. 6 above. Also in fig. 10b is shown the effects of allowing the virtuality of some links below the cutoff. Again the differences are small.

In fig. 10c we see the effect of different regularizations of the splitting functions. The line LDC E uses the fit E in the previous section, where all  $q \rightarrow q$  and most of the  $g \rightarrow q$  splittings are disallowed and all Sudakov form factors set to 1. For the final

state generation, all splittings are again included, and we see a clear enhancement w.r.t. the default LDC A strategy which includes Sudakov form factors. The line LDC A<sub>0</sub> uses the same parton densities as the default strategy, but excludes the Sudakov form factors when generating the final states. The main effect of the form factor is to scale down all weights, and since in the total number of events is fixed, the effects on the final state is small. The fact that LDC E is as different is then mostly due to the difference in the input parton densities.

Finally in fig. 10d, we show the effects of using different fitting procedures for the input parton densities and we see that the differences are small.

## 6 Conclusions

We have here presented the first implementation of the Linked Dipole Chain model in an event generator. Being based on the CCFM formalism it represents one of the first attempts to correctly describe the details of the hadronic final states in small- $x$  deep inelastic scattering to leading-log accuracy.

The LDC model was originally formulated only for  $g \rightarrow g$  splittings in a strict leading-log approximation. Going from this to a full event generator is not trivial, and we have here described how we implement massive quarks splittings, sub-leading corrections, convolution with input parton densities, energy and momentum conservation, Sudakov form factors, final-state radiation and hadronization.

Our implementation still suffers from some uncertainties. One is the input parton densities which are poorly constrained because only  $F_2$  data can be fitted, where the gluon only enters indirectly. Another issue is the uncertainty in how to deal with the final state of chains where a link drops below the cutoff, surrounded by one perturbative system on each side. But from the results in the previous sections, the main uncertainty is the regularization of the splitting functions and the conservation of total momentum in the evolved parton density functions. The correct way to treat this is with Sudakov form factors. But in the current implementation these are only treated in an approximate way and they need to be examined in more detail in the future.

Despite these uncertainties, the result presented here allows for some conclusions. Compared with the LEPTO event generator, which is based on DGLAP evolution, LDC is clearly better in describing the hadronic activity in the forward region at HERA at small  $x$ . The description is not perfect, however, and it seems that LDC is still underestimating the perturbative activity in the forward region.

We have also shown the relative importance between DGLAP-like chains with monotonically increasing virtualities and the unordered chains in the full LDC model, and

found that unordered chains indeed are very important, but that at HERA, most of the activity can be attributed to DGLAP-like chains where the link closest to the photon is allowed to be above  $Q^2$ .

The main goals for the future developments of the LDC generator is to investigate the exact form of the Sudakov form factors, and to include a treatment of hadron–hadron collisions, to get a better constraint on the input parton densities. Also further studies of the final state of chains with two or more perturbative systems connected with sub-cutoff links ought to be done. This is especially interesting in connection with the large fraction of rapidity-gap events found at HERA.

Despite the shortcomings of the current implementation, we feel that the LDC event generator may become a very important tool for understanding the small- $x$  hadronic final states at HERA.

## Acknowledgements

We would like to thank Bo Andersson and Gösta Gustafson for important contributions and discussions. We would also like to thank Hannes Jung for providing us with a preliminary HZTOOL implementation of the H1 results on di-jet production [30].

## References

- [1] V.N. Gribov, L.N. Lipatov, *Sov. J. Nucl. Phys.* **15** (1972) 438 and 675; G. Altarelli, G. Parisi, *Nucl. Phys.* **B126** (1977) 298; Yu.L. Dokshitzer, *Sov. Phys. JETP* **46** (1977) 641.
- [2] E.A. Kuraev, L.N. Lipatov and V.S. Fadin, *Zh. Eksp. Teor. Fiz.* **72** (1977) 373, *Sov. Phys. JETP* **45** (1977) 199; Ya.Ya. Balitsky and L.N. Lipatov, *Yad. Fiz.* **28** (1978) 1597, *Sov. J. Nucl. Phys.* **28** (1978) 822.
- [3] See eg. J. Blümlein et al., Proceedings of the “Future Physics at HERA” workshop, Hamburg 1996, eds. G. Ingelman, A. De Roeck and R. Klanner, vol. 1, p. 3, hep-ph/9609425 and references therein.
- [4] See eg. M. Erdmann et al., Proceedings of the “Future Physics at HERA” workshop, Hamburg 1996, eds. G. Ingelman, A. De Roeck and R. Klanner, vol. 1, p. 500, hep-ph/9610327 and references therein.
- [5] M. Ciafaloni, *Nucl. Phys.* **B269** (1988) 49; S. Catani, F. Fiorani, G. Machesini, *Phys. Lett.* **B234** (1990) 339, *Nucl. Phys.* **B336** (1990) 18.
- [6] G. Marchesini et al., *Comput. Phys. Comm.* **67** (1992) 465.

- [7] G. Ingelman, A. Edin and J. Rathsman, *Comput. Phys. Comm.* **101** (1997) 108, hep-ph/9605286.
- [8] H1 Collaboration, S. Aid et al., *Phys. Lett.* **B356** (1995) 118, hep-ex/9506012.
- [9] H1 Collaboration, C. Adloff et al., *Nucl. Phys.* **B485** (1997) 3, hep-ex/9610006.
- [10] L. Lönnblad, *Comput. Phys. Comm.* **71** (1992) 15.
- [11] B. Andersson et al., *Z. Phys.* **C43** (1989) 621.
- [12] G. Marchesini, B. Webber, *Nucl. Phys.* **B386** (1992) 215.
- [13] B. Andersson, G. Gustafson, J. Samuelsson, *Nucl. Phys.* **B463** (1996) 217.
- [14] G. Gustafson, *Phys. Lett.* **B175** (1986) 453;  
G. Gustafson, U. Pettersson, *Nucl. Phys.* **B306** (1988) 746;  
B. Andersson, G. Gustafson, L. Lönnblad, *Nucl. Phys.* **B339** (1990) 393.
- [15] B. Andersson et al., *Z. Phys.* **C71** (1996) 613.
- [16] H. Kharraziha, “The LDCMonte Carlo”, talk presented at the DIS '97 conference, Chicago, April 1997, to be published in the proceedings.
- [17] B. Andersson, G. Gustafson and H. Kharraziha,  
LU-TP 97-29, aps1997nov19\_001, hep-ph/9711403.
- [18] R.D. Peccei, R. Rückl, *Nucl. Phys.* **B162** (1980) 125;  
Ch. Rumpf, G. Kramer, J. Willrodt, *Z. Phys.* **C7** (1981) 337.
- [19] B. Andersson, P. Dahlqvist and G. Gustafson, *Phys. Lett.* **B214** (1988) 604;  
*Z. Phys.* **C44** (1989) 455.
- [20] L. Lönnblad, *Z. Phys.* **C70** (1996) 107.
- [21] T. Sjöstrand, *Comput. Phys. Comm.* **82** (1994) 74
- [22] H1 collaboration, S. Aid et al., *Nucl. Phys.* **B470** (1996) 3, hep-ex/9603004.
- [23] ZEUS collaboration, M. Derrick et al., *Z. Phys.* **C72** (1996) 399, hep-ex/9607002.
- [24] NMC collaboration, M. Arneodo et al., *Phys. Lett.* **B364** (1995) 107, hep-ph/9509406.
- [25] E665 collaboration, M.R. Adams et al., *Phys. Rev.* **D54** (1996) 3006
- [26] M. Glück, E. Reya and A. Vogt, *Z. Phys.* **C48** (1990) 471; *Z. Phys.* **C53** (1992) 127; *Z. Phys.* **C67** (1995) 433.
- [27] J. Bromley et al., Proceedings of the “Future Physics at HERA” workshop, Hamburg 1996, eds. G. Ingelman, A. De Roeck and R. Klanner, vol. 1, p. 611.
- [28] ZEUS Collaboration, M. Derrick et al., *Z. Phys.* **C70** (1996) 1, hep-ex/9511010.
- [29] EMC Collaboration, M. Arneodo et al., *Z. Phys.* **C36** (1987) 527.
- [30] H1 Collaboration, T. Ahmed et al., Contributed paper, Abstract 247, HEP97, Jerusalem, Israel, August 1997 (unpublished).
- [31] M. Kuhlen, *Phys. Lett.* **B382** (1996) 441
- [32] A. Edin, G. Ingelman, J. Rathsman, *Phys. Lett.* **B366** (1996) 371, hep-ph/9508386; *Z. Phys.* **C75** (1997) 57, hep-ph/9605281.

[33] H-U. Bengtsson, *Comput. Phys. Comm.* **31** (1984) 323.

[34] M.H. Seymour, *Nucl. Phys.* **B436** (1995) 443

## Appendix A: Colour connected matrix element corrections

We will here describe the splitting functions that are used for the local sub-collisions (see point 10 in section 3). These are derived from the corresponding *colour connected*  $2 \rightarrow 2$  QCD matrix elements presented in [33].

In order to use matrix elements for deriving splitting functions, it is necessary to take colour connections into account. We can illustrate this statement with the matrix element for the  $g + g \rightarrow q + \bar{q}$  process. Suppose we are in a frame where the incoming gluons are moving head on and parallel to the longitudinal axis and let  $\zeta_{+(-)}$  be the positive (negative) light-cone momentum fraction for the quark and  $\bar{\zeta}_{+(-)}$  be the same for the anti-quark. Because of symmetry between the quark and the anti-quark it is clear that the matrix element must be symmetric in these variables:  $|\mathcal{M}|^2(\zeta_{+(-)}, \bar{\zeta}_{+(-)}) = |\mathcal{M}|^2(\bar{\zeta}_{+(-)}, \zeta_{+(-)})$ . In the program, the colours are connected randomly so that e.g. the quark has the same probability to be connected with the gluon coming in from either the proton or the photon side. This would mean that the two diagrams a') and  in fig. 11 would be equally probable.

This is because the matrix element is calculated with an averaging of the colour states of the gluons. The corresponding colour connected matrix element,  $|\mathcal{M}_{cc}|^2$  is on the other hand calculated with the assumption that the colour states of the incoming gluons are known. This means that we get two separate contributions, one from the case that the quark is colour connected with the gluon coming in from one side, say the proton side, and one contribution from the case that it is connected with the gluon from the photon side. Each of these contributions is non-symmetric with respect to the quark and anti-quark variables, while the sum of them still is symmetric.

A similar procedure is used in the  $\mathcal{O}(\alpha\alpha_s)$  matrix element correction (see point 11 in section 3), to separate the  $\gamma g$  matrix element into two contributions corresponding to quark and anti-quark scattering respectively as described in ref. [34].

For a colour connected matrix element  $|\mathcal{M}_{cc}|^2(\hat{s}, \hat{t}, \hat{u})$ , the corresponding splitting function is given by the formula

$$P(z) \propto z(1-z) \cdot |\mathcal{M}_{cc}|^2(1, z, 1-z) \quad \text{with } z = z_+ \approx z_- \quad (25)$$

The splitting functions  $\mathcal{P}_{ijk}(z)$  where the colour factor is divided out and with the

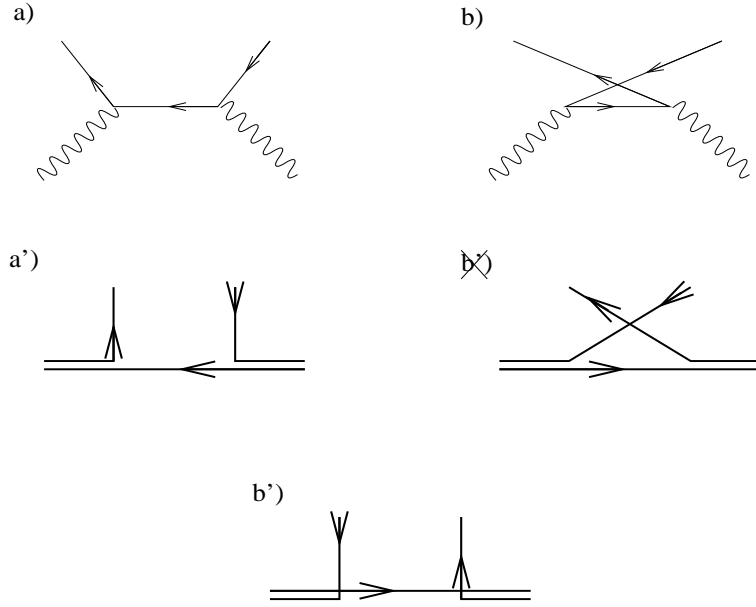


Figure 11: *Feynman vs. colour connection diagrams for the  $g + g \rightarrow q + q$  subprocess. If we do not average the colour states, the diagrams  $a')$  and  $b')$  give separate contributions. The contribution from diagram  $b')$  should be suppressed.*

successive flavours  $ijk$  for the propagators, become

$$\begin{aligned}
 \mathcal{P}_{qqq}(z) &= (1-z)^2 [z^2 + (1-z)^2] \\
 \mathcal{P}_{qqg}(z) = \mathcal{P}_{gqq}(z) &= 0 \\
 \mathcal{P}_{qgq}(z) &= \frac{1-z}{z} [1 + (1-z)^2] \\
 \mathcal{P}_{gqg}(z) &= (1-z)^2 [z^2 + (1-z)^2] \\
 \mathcal{P}_{qgg}(z) = \mathcal{P}_{ggq}(z) &= \frac{1}{2z} [1 + (1-z)^2]^2 \\
 \mathcal{P}_{ggg}(z) &= \frac{1}{3} \left\{ \frac{[1-z(1-z)]^2}{z(1-z)} \cdot \theta(0.5-z) + 2 \frac{1-z}{z} [1-z+z^2]^2 \right\}.
 \end{aligned} \tag{26}$$

The  $\theta$ -function in the first term of  $\mathcal{P}_{ggg}$  is a cut-off to prevent divergences. This is needed since the Sudakov form factors that are used regularize only regions with ordered virtualities. The splitting functions  $\mathcal{P}_{qqg}$  and  $\mathcal{P}_{gqq}$  are set to zero since they correspond to the same  $(g + q \rightarrow g + q)$  scattering as the splitting functions  $\mathcal{P}_{qgg}$  and  $\mathcal{P}_{ggq}$  which have been chosen to take the whole contribution.

Here we have summed the contributions from different colour connections for each flavour combination. The choice of colour connections has an effect on the multiplicity and transverse momentum distributions at the hadronic level. Therefore, we will

in the future use this information also to choose the colour connections for the local sub-collisions.